The importance of turbulent ocean-sea ice nutrient exchanges for simulation of ice algal biomass and production with CICE6.1 and Icepack 1.2

Pedro Duarte[1], Philipp Assmy[1], Karley Campbell[2,3], Arild Sundfjord[1]

[1] Norwegian Polar Institute, Fram Centre, Tromsø, Norway

[2] Department of Arctic and Marine Biology, UiT The Arctic University of Norway, Norway

[3] Bristol Glaciology Centre, University of Bristol, UK

Correspondence to: Pedro Duarte (Pedro.Duarte@npolar.no)

Abstract. Different sea-ice models apply unique approaches in the computation of nutrient diffusion between the ocean and the ice bottom, which are generally decoupled from the calculation of turbulent heat flux. Often, a simple molecular diffusion formulation is used. We argue that nutrient transfer from the ocean to sea ice should be as consistent as possible with heat transfer, since all these fluxes respond to varying forcing in a similar fashion. We hypothesize that biogeochemical models which do not consider such turbulent nutrient exchanges between the ocean and the sea-ice, despite considering brine drainage and bulk exchanges through ice freezing/melting, may underestimate bottom-ice algal production. The Los Alamos Sea Ice Model (CICE + Icepack) was used to test this hypothesis by comparing simulations without and with diffusion of nutrients across sea-ice bottom dependent on velocity-shear, implemented in a way that is consistent with turbulent heat exchanges. Simulation results support the hypothesis, showing a significant enhancement of ice algal production and biomass when nutrient limitation was relieved by bottom-ice turbulent exchange. Our results emphasize the potentially critical role of turbulent exchanges to sea ice algal blooms, and the importance of thus properly representing them in biogeochemical models. The relevance of this becomes even more apparent considering ongoing trends in the Arctic Ocean, with a predictable shift from light to nutrient limited growth of ice algae earlier in the spring, as the sea ice becomes more fractured and thinner with a larger fraction of young ice with thin snow cover.

1 Introduction

Momentum, heat and mass fluxes between the ocean and the sea-ice are of utmost importance to predict sea-ice motion, thermodynamics, and biogeochemistry. However, when we look at models released over the last decades, we find not only inter-model differences in the physical concepts used to describe the processes responsible for some of the above fluxes, but also intra-model differences in the approaches used in calculating, for example, heat and mass fluxes. In this work we will focus on the differences related with the vertical diffusion of tracers between the water column and the bottom-ice and attempt to explore their consequences on nutrient limitation for sea-ice algal growth.

We may divide the ocean-ice exchange processes into those related to: (i) entrapment during freezing; (ii) flushing and release during melting;(iii) brine gravity drainage, driven by density instability, parameterized as either a diffusive or a convective process; (iv) molecular diffusion; and (v) turbulent diffusion at the interface between the ocean and the ice induced by velocity shear – the latter process being the focus of this study (e.g. Arrigo et al, 1993 and references therein; Jin et al., 2006; McPhee, 2008; Notz and Worster, 2009; Turner et al., 2013; Tedesco and Vichi, 2010, 2019; Jeffery et al., 2011; Vancoppenolle et al., 2013).

These processes are considered is several sea ice models. Arrigo et al. (1993) distinguished nutrient exchanges resulting from gravity drainage in brine channels, from brine convection in the skeletal layer, dependent on the ice growth rate. These brine fluxes were used to calculate nutrient exchanges as a diffusive process. Lavoie et al. (2005) also calculated nutrient exchanges as a diffusive process. Jin et al. (2006; 2008) computed nutrient fluxes across the bottom layer as an advection process dependent on ice growth rate and based on Wakatsuchi and Ono (1983). Molecular diffusion was also considered. More recently, other authors have integrated formulations of "enhanced diffusion" (Vancoppenolle et al., 2010; Jeffery et al., 2011) or convection (Turner et al., 2013), based on hydrostatic instability of brine density profiles, to compute brine gravity drainage and tracer exchange within the ice and between the ice and the sea water. Comparisons between salt dynamics in growing sea ice with salinity measurements showed that convective Rayleigh number-based parameterizations (e.g. Wells et al., 2011), such as the one by Turner et al. (2013), outperform diffusive and simple convective formulations (Thomas et al., 2020).

Interestingly, heat exchange is often calculated differently from salinity in models. In the case of the former, typically, a transfer mechanism (turbulent or not) at the interface between the ocean and the sea ice is not dependent on any type of brine exchange. In the case of salinity, such a mechanism is not considered (e.g. Vancoppenolle et al., 2007; Turner et al., 2013). Presumably, such differences result from the relative importance of various physical processes for different tracers. Heat transfer between the ice and the water is a fundamental mechanism in explaining sea-ice thermodynamics, irrespective of brine exchanges. On the other hand, ice desalination depends mostly on brine gravity drainage and flushing during melting (Notz and Worster, 2009).

Vertical convective mixing of nutrients under the sea ice may result from brine rejection and/or drainage from the sea ice (Lake and Lewis, 1970; Niedrauer and Martin, 1979; Reeburgh, 1984) and from turbulence due to shear instabilities generated by drag at the interface between the ocean and the sea ice (Gosselin et al., 1985; Cota et al., 1987; Carmack, 1986), internal waves and topographical features (Ingram et al., 1989; Dalman et al., 2019). Gosselin et al. (1985) and Cota et al. (1987) stressed the significance of tidally induced mixing in supplying nutrients to sympagic algae. Biological demand for silicic acid (hereafter abbreviated as silicate) and nitrate is limited by the physical supply (Cota and Horne, 1989; Cota and Sullivan, 1990).

The analysis of several models published over the last decades and their approaches to calculate tracer diffusion across the ice-ocean interface shows that some models do not consider this process or limit it to molecular diffusion. Other models consider turbulent exchanges parameterized as a function of the Rayleigh number, calculated from brine vertical density gradients. Only ~~one~~ two of the sampled models (Lavoie et al., 2005 and Mortenson et al., 2017) use~~s~~ ~~a~~ parameterizations based on friction velocity. The former uses eddy diffusion to simulate the vertical supply of nutrients to the molecular sublayer, where nutrient

fluxes and their supply to the bottom ice are limited by molecular diffusion. The latter uses a coupled ocean-sea ice model but, ultimately, molecular diffusion is the controlling process. Both authors use the same approach to compute the thickness of the molecular sublayer, based on friction velocity.

In the absence of ice growth and when brine gravity drainage is limited, diffusive nutrient exchanges between the ocean and the ice have the capacity to limit primary production. This limitation will be alleviated in the presence of a turbulent exchange mechanism. We argue that nutrient transfer at the interface between the ocean and the sea ice should be as consistent as possible with heat transfer since all these fluxes are closely linked. We hypothesize that models which do not consider the role of current velocity shear on turbulent nutrient exchanges between the ocean and the sea-ice may underestimate bottom-ice algal production.

To test the above hypothesis, we use a 1D vertically resolved model implemented with CICE+Icepack and contrast results using the default diffusion parameterization and a "turbulent" parameterization analogous to that of heat and salt transfer, at the interface between the ocean and the sea ice, based on McPhee (2008). This implementation of the turbulent parameterization is specific for the software used and it may be different in other models.

2 Methods

2.1 Concepts

Turbulent exchanges may be parameterized through the flux of a quantity at the interface between the ocean and the sea ice, calculated as the product of a scale velocity and the change in the quantity from the boundary to some reference level (McPhee, 2008):

$$\langle w'S' \rangle = \alpha_s u^* (S_w - S_0) \qquad (1)$$

Where, $\langle w'S' \rangle$ represents the averaged co-variance of the turbulent fluctuations of interface vertical velocity (m s^{-1}) and salinity, respectively, α_s is an interface salt/nutrient exchange coefficient (dimensionless); u^* is the friction velocity (m s^{-1}); S_0 and S_w are interface and far-field salinities, respectively.

We calculate ~~salt or~~ nutrient exchanges using a similar approach:

$$F_N = -\alpha_s u^* (N_w - N_0) \qquad (\cancel{3}2)$$

~~In fact, t~~This is an extension of the concept used for heat and salt by McPhee (2008) (see page 112, Fig. 6.3). The minus sign used in (~~3~~2) ~~and (4)~~ is for compatibility with the CiCE + Icepack convention that upward fluxes are negative (e.g. Hunke et al., 2015). α_s varies between 8.6 10^{-5} , during the melting season, and 0.006, during winter (McPhee et al., 2008).

~~Where, <w'S'> represents the averaged co-variance of the turbulent fluctuations of interface vertical velocity (m s^{-1}) and salinity, respectively, α_s is an interface salt/nutrient exchange coefficient (dimensionless); u^* is the friction velocity (m s^{-1}); S_o and S_w are interface and far-field salinities, respectively.~~

~~Hereafter we will assume that salt turbulent exchanges are similar to nutrient exchanges and governed by the same principles and parameters. The main difference between turbulent heat and salt/nutrient exchanges is due to the exchange coefficients that may be higher for heat. The heat exchange coefficient (α_h) is around 0.006. The ratio (R) between α_h and α_s may vary from unity to a range between 35 and 70 during ice melting and because of double diffusion, leading to a range in α_s between 8.6 10^{-5} and 0.006 (McPhee et al., 2008).~~

~~The net downward heat flux from the ice to the ocean in the Los Alamos Sea Ice Model (CICE + Icepack) is given by (Hunke et al., 2015) and it is computed according to McPhee et al. (2008) [Eq. (2)]:~~

$$F_{bot} = -\rho_w c_w \alpha_h u^* (T_w - T_f) \quad (2)$$

~~Where, ρ_w is the density of seawater (kg m^{-3}); c_w is the specific heat of seawater (J kg^{-1} K^{-1}); α_h is the heat transfer coefficient (dimensionless); T_w is the water temperature (K); T_f if the freezing temperature (K).~~

~~We calculate salt or nutrient exchanges using a similar approach:~~

$$F_N = -\alpha_s u^* (N_w - N_0) \quad (3)$$

~~In fact, this is an extension of the concept used for heat and salt by McPhee (2008) (see page 112, Fig. 6.3). The minus sign used in (3) and (4) is for compatibility with the CICE + Icepack convention that upward fluxes are negative (e.g. Hunke et al., 2015).~~Before explaining how 3 was implemented in the CICE+Icepack we describe the model vertical biogeochemical grid (biogrid), the tracer equation and the bottom boundary conditions. The biogrid is the non-dimensional grid used for discretizing the vertical transport equations of biogeochemical tracers, defined between the brine height (h), which takes the value zero, and the ice-ocean interface, which takes the value one (Jeffery et al., 2016). The Icepack tracer equation (without biogeochemical reaction terms for the sale of simplicity) may be written as [for more details, refer Jeffery et al. (2011; 2016)]:

$$\varphi \frac{\partial N}{\partial t} = \left\{ \frac{(x-1)}{h} \frac{\partial z_t}{\partial t} - \frac{x}{h} \frac{\partial z_b}{\partial t} \right\} \frac{\partial}{\partial x} (\varphi N) + \frac{1}{h} \frac{\partial}{\partial x} (w_f N) + \frac{\partial}{\partial x} \left(\frac{D_{MLD} + \varphi D_m}{h^2} \frac{\partial N}{\partial x} \right) \quad (3)$$

Where $0 \leq x \leq 1$ is the relative depth of the vertical domain of the biogrid, z_t and z_b are vertical positions of the ice top and bottom (m), respectively, φ is sea ice porosity, w_f is the Darcy velocity due to the sea ice flushing of tracers (m s^{-1}), ~~Where~~ D_m is the molecular diffusion coefficient and D_{MLD} is the mixed length diffusion coefficient (m^2 s^{-1})~~ (Jeffery et al., 2011)~~. D_{MLD} is detailed in Jeffery et al. (2011) and it is zero when the brine vertical density gradient is stable, otherwise (when density increases towards the ice top) it is calculated as:

$$D_{MLD} = \frac{gk}{\mu} \Delta\rho_e l \quad (4)$$

Where g is the acceleration of gravity (9.8 m s^{-2}), k is sea ice permeability, μ is dynamic viscosity (2.2 kg m^{-1}s^{-1}), ρ_e is the equilibrium brine density and l is a length scale (7 m). The values shown here are the default ones in CICE+Icepack.

Formatted: Font: Italic

The bottom boundary condition of 3 is based on values of N at the sea ice bottom interface (N_0 at $x=1$) and in the ocean (N_w) (Jeffery et al., 2011), Therefore, the last term of equation 3 at the bottom boundary may be written as:

$$\frac{D_{MLD}+\varphi D_m}{h^2 \partial x}(N_0 - N_w) \quad (5)$$

With $\phi=1$.

In CICE+Icepack, diffusion time scales are calculated separately for later usage in 3 as:

$$\tau = \frac{D_m}{h^2}[s^{-1}] \quad (6)$$

And

$$\tau = \frac{D_{MLD}}{h^2}[s^{-1}] \quad (7)$$

A~~A~~ similar timescale for the~~is~~ turbulent process described by equation 3 may be calculated from:

~~Therefore, in the CICE model the implementation of turbulent diffusion nutrient exchanges at the ice-ocean interface in terms consistent with heat exchanges is quite straightforward, depending on changing the timescales from Eq. (5) to (4). In other models, other approaches may be required.~~

$$\tau = \frac{\alpha_s u^*}{\cancel{z}h}[s^{-1}] \quad (\cancel{4}8)$$

Therefore, in the Los Alamos Sea Ice Model the implementation of turbulent diffusion nutrient exchanges at the ice-ocean interface is quite straightforward. In other models, other approaches may be required.

~~Where z is a vertical distance (m) (h in the Los Alamos Sea Ice Model, see below). The above time scale is calculated for consistency with CICE implementation of diffusion, where a comparable time scale is calculated as:~~

$$\cancel{\tau = \frac{D_m}{h^2}[s^{-1}] \quad (5)}$$

~~Or~~

$$\cancel{\tau = \frac{D_{MLD}}{h^2}[s^{-1}] \quad (6)}$$

The usage of h in these timescales implies merely the way they are normalized in the code before the actual diffusive fluxes are calculated considering the distance between the points ($h.\partial x$, see above equation 3) where variables are calculated, along the layers of the biogrid. The product $h.x$ corresponds to the actual distance of a given point from the top of the biogrid.

In the simulations using turbulent diffusion, we perform the same calculations, except that the molecular diffusion term $\frac{\varphi D_m}{h^2}$ is replaced with a turbulent diffusion term $\frac{\alpha_s u^*}{h}$ at the interface between the last model layer and the ocean. This exchange process takes place "outside" the sea ice where $\phi=1$, affecting directly only the tracer concentration at the ice-ocean interface.

Formatted: Font: Italic

Formatted: Font: Italic

Formatted: Font: Italic, Lowered by 3 pt

Formatted: Font: Italic

Formatted: English (United States)

Formatted: English (United States)

Formatted: English (United States)

~~Where D_m is the molecular diffusion coefficient and D_{MLD} is the mixed length diffusion coefficient ($m^2 s^{-1}$) (Jeffery et al., 2011).~~

~~In the Los Alamos Sea Ice Model, h corresponds to the thickness of the biogeochemical grid (biogrid). This is the non-dimensional grid used for discretizing the vertical transport equations of biogeochemical tracers, defined between the brine height, which takes the value zero, and the ice-ocean interface, which takes the value one (Jeffery et al., 2016). The usage of h in these timescales implies merely the way they are normalized in the code before the actual diffusive fluxes are calculated considering the distance between the points ($h.\partial x$, see below equation 7) where variables are calculated, along the layers of the biogrid. The product $h.x$ corresponds to the actual distance of a given point from the top of the biogrid. The time scales expressed in equations 5 and 6 are included in the Icepack transport equation, which may be written as [for more details, refer Jeffery et al. (2011; 2016)]:~~

$$\varphi \frac{\partial N}{\partial t} = \left(\frac{(x-1)}{h}\frac{\partial z_t}{\partial t} - \frac{x}{h}\frac{\partial z_b}{\partial t}\right)\frac{\partial}{\partial x}(\varphi N) + \frac{1}{h}\frac{\partial}{\partial x}(w_f N) + \frac{\partial}{\partial x}\left(\frac{D_{MLD}+\varphi D_m}{h^2}\frac{\partial N}{\partial x}\right) \quad (7)$$

~~Where $0 \leq x \leq 1$ is the relative depth of the vertical domain of the biogrid, z_t and z_b are vertical positions of the ice top and bottom (m), respectively, φ is sea ice porosity, w_f is the Darcy velocity due to the sea ice flushing of tracers ($m\ s^{-1}$). D_{MLD} is detailed in Jeffery et al. (2011) and it is zero when the brine vertical density gradient is stable, otherwise (when density increases towards the ice top) it is calculated as:~~

$$D_{MLD} = \frac{gk}{\mu}\Delta\rho_e l \quad (8)$$

~~Where g is the acceleration of gravity ($9.8\ m\ s^{-2}$), k is sea ice permeability, μ is dynamic viscosity ($2.2\ kg\ m^{-1}s^{-1}$), ρ_e is the equilibrium brine density and l is a length scale (7 m). The values shown here are the default ones in Icepack.~~

~~The last term of equation 7 includes the contribution of molecular diffusion that is calculated at the interface of all layers of the biogrid and at the interface of the last layer and the ocean. In the simulations using turbulent diffusion, we perform the same calculations, except that the molecular diffusion term $\frac{\varphi D_m}{h^2}$ is replaced with a turbulent diffusion term $\frac{\alpha_s u^*}{h}$ at the interface between the last model layer and the ocean.~~

~~The transport equation is resolved along the biogrid, with a Flux-Corrected, Positive Definite Transport Scheme, using the finite element Galerkin discretization (Jeffery et al., 2016). In the case of the bottom ice layer, tracer concentrations are calculated at the ice-ocean interface.~~

~~Therefore, in the CICE model the implementation of turbulent diffusion nutrient exchanges at the ice-ocean interface in terms consistent with heat exchanges is quite straightforward, depending on changing the timescales from Eq. (5) to (4). In other models, other approaches may be required.~~

From equations ~~4~~ 6 - ~~6~~ 8 it turns out that the product $\alpha_s u$ by distance (z) has the same dimensions of D_m *or* D_{MLD}, corresponding to a turbulent diffusion coefficient. Assuming $z \approx 0.01$ m, turbulent diffusion induced by velocity shear~~,~~ becomes comparable with molecular diffusion only for $u^* < 0.0012$ m s^{-1}, considering the lower end of the α_s range (8.6 10^{-5}, see above) or $u^* < 1.7$ 10^{-5} m s^{-1}, considering the upper end of the α_s range (0.006). If we assume instead $z \approx$ 0.00054 m [the average thickness of the

molecular sublayer reported in Lavoie et al. (2005)]~~0.001 m~~, the calculated $u*$ values increase by one-two orders ~~one order~~ of magnitude (depending on α_s) but are still ~~very~~ low (0.0004-0.03 m s^{-1}). In fact, such low friction velocities would require ~~extremely~~ low "stream" velocities - relative ice-ocean velocities. For an account of the relationship between "stream" and friction velocities under the sea ice see Supplementary information 3 of Olsen et al. (2019) and references therein. These authors show that "stream" velocities of only a few centimetres per second lead to friction velocities one order of magnitude lower but still in the order of 0.001 ms^{-1}, i.e., ~~comparable~~ larger only ~~to~~ than the highest $u*$ values estimated above. Considering current velocities relative to the sea ice observed during the N-ICE2015 cruise [Granskog et al., 2018; Figure 2d of Duarte et al. (2017)], with most values between 0.05 and > 0.2 m s^{-1}, it is rather likely that friction velocities under the ice are frequently above the thresholds calculated above and that turbulent diffusion will dominate over molecular diffusion. Dalman et al. (2019) provided experimental evidence for such turbulent nutrient fluxes to the ice bottom, leading to increased chlorophyll concentrations at the bottom ice, in a strait with strong tidal currents. The mechanism treated here as turbulent diffusion seems analogous to "forced convection" in the lowermost parts of the brine network, which is driven by pressure differences caused by the shear under the sea ice (Neufeld, 2008; Vancoppenolle et al., 2013).

2.2 Implementation

We used the Los Alamos Sea Ice Model, which is managed by the CICE Consortium with an active forum (https://bb.cgd.ucar.edu/cesm/forums/cice-consortium.146/) and a git repository (https://github.com/CICE-Consortium). It includes two independent packages: CICE and Icepack. The former computes ice dynamic processes and the latter ice column physics and biogeochemistry. Their development is handled independently with respect to the GitHub repositories (https://github.com/CICE-Consortium). All the changes described below were implemented in two forks to the above repository, one for Icepack and another for CICE and they may be found in Duarte (2021a and b, respectively).

Our simulations may be run using only Icepack, since they are focused on ice column physics and biogeochemistry, without the need to consider ice dynamic processes. However, we used both CICE + Icepack together to allow for use of netCDF based input/output not included in Icepack. Therefore, we defined a 1D vertically resolved model with 1 snow layer and 15 ice layers and 5X5 horizontal cells. This is the minimum number of cells allowable in CICE due to the need to include halo cells (only the central "column" is simulated). Therefore, ice column physics and biogeochemistry were calculated by Icepack but CICE was the model driver. The input file (ice_in) used in this study was included in our CICE fork and it lists all parameters used in the model and described in Hunke et al. (2016), Jeffery et al. (2016), Duarte et al. (2017) and in Tables S1 and S2. Any changes in "default" parameters or any other model settings will be specified.

We made several modifications in CICE to allow using forcing time series collected during the Norwegian young sea ice (N-ICE2015) expedition (Granskog et al., 2018) and described in Duarte et al. (2017) (see Fig. 2 of the cited authors). These modifications were meant to allow reading of forcing data at higher frequencies than possible with the standard input subroutines in the CICE file ice_forcing.F90.

When the dynamical component of CICE is not used, u* is set to a minimum value instead of being calculated as a function of ice-ocean shear stress (Hunke et al., 2015). Duarte et al. (2017) implemented shear calculations from surface current velocities (one of the models forcing functions) irrespective of the use of the CICE dynamics code. These modifications were also incorporated in the current model configuration so that shear can be used to calculate friction velocity and, thereafter, influence heat and tracer/nutrient exchanges, following Eqs. (~~3~~1) and (~~4~~8) and parameters described in McPhee et al. (2008). When the parameter kdyn is set to zero in ice_in, ice dynamics is not computed, but shear is calculated in the modified subroutine icepack_step_therm1, file icepack_therm_vertical.F90. If kdyn is not zero, these calculations are ignored since shear is already calculated in the dynamical part of the CICE code.

A Boolean parameter (Bottom_turb_mix) was added to the input file, which is set to "false" or "true" when the standard molecular diffusion approach or the new turbulent based diffusion approach is used, respectively. Another Boolean parameter (Limiting_factors_file) was added to the ice_in file. When set to "true" limiting factor values for light, temperature, nitrogen, and silicate are written to a text file every model timestep. These are calculated by Icepack biogeochemistry, according to Jeffery et al. (2016), but there is no writing-output option in the standard code.

2.3 Model simulations

Simulations were run for a refrozen lead (RL) without snow cover and for second-year sea ice (SYI) with ~40 cm snow cover monitored in April-June during the N-ICE2015 expedition (Granskog et al., 2018 and Fig. 1 of Duarte et al. 2017). Details on model forcing with atmospheric and oceanographic data collected during the N-ICE2015 expedition, including citations and links to the publicly available datasets are given in Fig. 2 and section 3 of Duarte et al. (2017) and in the Supporting information file. These data sets include wind speed, air temperature, precipitation, and specific humidity (Hudson et al., 2015); incident surface short and longwave radiation (Hudson et al., 2016); ice temperature and salinity (Gerland et al., 2017); sea surface current velocity, temperature, salinity and heat fluxes from a turbulence instrument cluster (TIC) (Peterson et al., 2016); sea surface nutrient concentrations (Assmy et al., 2016) and sea ice biogeochemistry (Assmy et al., 2017). Ocean forcing is based on measurements within the surface 2 meters which provide the boundary condition for the sea ice model. Model forcing files may be found in Duarte (2021c).

Refrozen lead simulations started with zero ice, whereas Second Year Ice Simulations started with initial conditions described in the Supporting information file (Table S3).

We ran simulations with the standard formulations for biogeochemical processes described in Jeffery et al. (2016) and settings described in Duarte et al. (2017), using mushy thermodynamics, vertically resolved biogeochemistry, and including: freezing, flushing, brine mixed length and molecular diffusion within the ice and at the interface between the ocean and the sea ice as nutrient exchange mechanisms (Jeffery et al., 2011, 2016). We contrasted the above simulations against others that replaced brine molecular and mixed length diffusion of nutrients at the interface between the ocean and the sea ice with diffusion driven by current velocity shear (Table 1), calculated similar to heat exchanges, and following the parameterization described in McPhee et al. (2008) and detailed above (equations 2 - 7). This contrast provides insight into the effects of velocity shear on

nutrient diffusion, ice algal production (mg C m^{-2} d^{-1}), chlorophyll standing stocks (mg *Chl a* m^{-2}) and vertical distribution of chlorophyll concentration (mg *Chl a* m^{-3}) [note that CICE model output for algal biomass in mmol N m^{-3} was converted to mg *Chl a* m^{-3} as in Duarte et al. (2017), using 2.1 mg *Chl a* mmol N^{-1} and following Smith et al. (1993)]. However, due to the concurrent effects of algal biomass exchange between the ocean and ice, such a contrast is not enough to explicitly test our hypothesis and conclude about the effects of turbulent-driven nutrient supply on ice algal nutrient limitation. Therefore, simulations were also run contrasting the same model setups, as described above, but restarting from similar algal standing stocks and vertical distributions within the ice and, switching off algal inputs from the water to the ice. This was done by nullifying the variable algalN, defining the ocean surface background ice algal concentration, in file icepack_zbgc.F90, subroutine icepack_init_ocean_bio and in the restart files. In the case of the RL simulations that started with zero ice, first a simulation was run until the 12 May, and then the obtained ice conditions were used to restart new simulations without algal inputs from the ocean (algalN = 0 mmol N m^{-3}). This way, when the simulations restarted, there was already an ice algal standing stock necessary for the modelling experiments developed herein. The SYI simulations were, by default, "restart simulations", beginning with observed ice physical and biogeochemical variables. Therefore, there was already an algal standing stock in the ice from the onset (Text S1 and Table S3).

McPhee et al. (2008) estimated different values for α_s depending on whether the sea ice is growing (highest value) or melting (lowest value) (Table 1). When running simulations for the RL, in some cases, we used only the minimum or the maximum values for α_s to allow for a more extreme contrast between molecular and turbulent diffusion parameterizations. This was done since the former value will tend to minimize differences, whereas the latter will tend to emphasize them. We also completed simulations for the RL and for SYI changing between the maximum and the minimum values of α_s, when ice was growing or melting, respectively, and following McPhee et al. (2008) (see Table 1 for details). This parameterization with a variable α_s is likely the most realistic one, accounting for double diffusion during ice melting (McPhee et al., 2008).

Apart from contrasting the way bottom-ice exchanges of nutrients were calculated, some simulations contrasted different parameters related to silicate limitation (Table 1). This approach follows Duarte et al. (2017), where simulations were tuned by changing the Si:N ratio and the half saturation constant for silicate uptake because silicate limitation was leading to an underestimation of algal growth. From this exercise we were able to assess if such tuning was still necessary after implementing turbulent diffusion at the interface between the ocean and the sea ice, driven by velocity shear. Moreover, we repeated simulations with varying snow heights to further investigate the interplay between light and nutrient limitation under contrasting nutrient diffusion parameterizations (Table 1).

Table 1. Model simulations. Refrozen lead (RL) simulation RL_Sim1 corresponds to RL_Sim5 described in Duarte et al. (2017) - the simulation leading to a best fit to the observations in that study. The remaining RL simulations 2 – 5 differ from RL_Sim1 in using turbulent diffusion at the interface between the ocean and the sea ice for nutrients in a comparable way as it is calculated for heat and driven by velocity shear. Moreover, RL_Sim5 differs in the concentration of ice algae in the water column that colonize the sea ice bottom (algalN) and in silicate limitation related parameters. These changes were done iteratively to fit the model to the observations. In RL_Sim2 and RL_Sim3 the maximum (α_s=*0.006*) and the minimum (α_s=*0.006/70=8.6 10*$^{-5}$) values recommended by McPhee et al. (2008), respectively, are used throughout the simulations, to provide extreme case scenarios for comparison with RL_Sim1. In RL_Sim4, α_s=*8.6 10*$^{-5}$when ice is not growing and *0.006* otherwise, as recommended by McPhee et al. (2008), to account for double diffusive processes during ice melting that slow down mass exchanges. The remaining RL simulations (R__Sim6-9) are like the previous ones (RL_Sim1-4, respectively), except for algalN that was set to zero mmol N m^{-3}, and all simulations were restarted with the same values for all variables. Therefore, simulations 6 – 9 may differ only from 13 May 2015, when they were restarted. Second year ice simulation SYI_Sim_1 is based on Duarte et al. (2017) SYI_Sim4 but without algal motion. SYI_Sim2 and SYI_Sim3 use turbulent diffusion at the interface between the ocean and the sea ice. The former uses a decreased half saturation constant for silicate uptake, just like SYI_Sim1, whereas the latter uses the standard CICE value. The remaining SYI simulations (SYI__Sim4 and 5) are like SYI_Sim1and 2, except for algalN that was set to zero. Simulations SYI_Sim1 and SYI_Sim2 were repeated but with different initial snow thickness of 30, 20 and 15 cm to further investigate the interplay between light and silicate limitation (see text). Modified parameter values from one simulation to the next are marked in bold, separately for RL and SYI simulations. Modified parameters are based on literature ranges [e.g. Brzezinski (1985) and Hegseth (1992), for ratio_Si2N_diatoms, Nelson and Treguer (1992), for K_Sil_diatoms], Urrego-Blanco et al. (2016), for R_snw], or on previous model calibration work (Duarte et al., 2017). Parameters values were modified in the model input file ice_in, except for algalN and α_s, that are hard-coded.

Simulations	**Modified parameters (bold types below indicate the parameter abbreviation used in Icepack)**					
	Silica to nitrogen ratio in diatoms (**ratio_Si2N_diatoms**)	Half saturation constant for silicate uptake (**K_Sil_diatoms**, mM Si)	Ice algal concentration in the water (**algalN**, mM N)	Boolean to define the usage of either molecular (0) or turbulent diffusion (1) (Bottom_turb_mix)	Interface salt/nutrient turbulent exchange coefficient (α_s)	Sigma coefficient for snow grain (**R_snw**)
RL_Sim1	1.0	2.2	11 10^{-4}	0	-	1.5
RL_Sim2	1.0	2.2	11 10^{-4}	**1**	**0.006**	1.5
RL_Sim3	1.0	2.2	11 10^{-4}	1	**8.6 10^{-5}**	1.5
RL_Sim4	1.0	2.2	11 10^{-4}	1	**8.6 10^{-5}-0.006**	1.5
RL_Sim5	**1.7**	**5.0**	**4 10^{-4}**	1	8.6 10^{-5}-0.006	1.5
RL_Sim6-9	As RL_Sim1-RL_Sim4, respectively		0	As RL_Sim1-RL_Sim4, respectively		
SYI_Sim1	1.0	2.2	11 10^{-4}	0	-	0.8

SYI_Sim2	1.0	2.2	11 10^{-4}	**1**	**8.6 10^{-5}-0.006**	0.8
SYI_Sim3	1.0	**4.0**	11 10^{-4}	1	8.6 10^{-5}-0.006	0.8
SYI_Sim4 and 5	As SYI_Sim1 and SYI_Sim2, respectively		0	As SYI_Sim1 and SYI_Sim2, respectively		

3. Results

The results of the simulations listed in Table 1 and presented below may be found in Duarte (2021d).

3.1 Refrozen lead simulations

All simulations with turbulent diffusion (RL_Sim2 – RL_Sim5, Table 1), predict higher bottom chlorophyll *a* (*Chl a*) concentration than with the standard molecular diffusion formulation (RL_Sim1) (Fig. 1a). Simulations RL_Sim2 - 4 grossly overestimate observations. Simulation RL_Sim3, using the lowest value for α_s, is closer both to observations and to RL_Sim1, as well as RL_Sim5, with the latter having the same α_s values of RL_Sim4 but a half saturation constant for silicate limitation increased from its tuned value in Duarte et al. (2017) of 2.2 μM to 5.0 μM and algalN reduced (Table 1) to bring model results closer to observations. Patterns between simulations for the whole ice column and considering both standing stocks and net primary production, are similar to those observed for the bottom-ice (Fig. 1b). Algal biomass is concentrated at the bottom layers (Fig. 2). Concentrations in the layers located between the bottom and the top of the biogrid, defined by the vertical extent (brine height) of the brine network (green lines in the map plots) (Jeffery et al., 2011) are < 10 mg *Chl a* m^{-3}. Ice thickness, temperature and salinity profiles are extremely similar among these simulations (Figs. S1 and S2).

Results for the silicate and nitrogen limiting factors are based on brine concentrations. Limiting factors exhibiting lower values (more limitation) in RL simulations are silicate, followed by light (Figs. 3, S3 – S5). Limiting values for silicate range between zero (maximum limitation) and one (no limitation), with stronger limitation after May 13 in all simulations (Fig. 3). The most severe silicate limitation is for RL_Sim1, where values drop to near zero around middle May. Despite the high average bottom *Chl a* concentration predicted in all simulations the bottom layer is where silicate limitation is less severe after May 13. This is more evident in simulations with turbulent bottom diffusion, where light limitation at the bottom-ice becomes more severe than silicate limitation around the end of May (Fig. S6).

Results obtained with RL_Sim6-9, without algal exchanges between the ocean and the ice (see Table 1), show similar patterns of those observed with RL_Sim1-5, respectively (Fig. 4 versus Fig. 2, Fig. S9 versus Fig. 3, Figs. S7 and S8 versus Figs. S1 and S2, Figs. S10 – S12 versus Figs. S3 – S5).

Interface diffusivity (one of CICE diagnostic variables, corresponding to the diffusion coefficient between adjacent biogeochemical layers and between the bottom layers and the ocean) for simulations with turbulent exchanges ($\alpha_s u^* H$) are up to two orders of magnitude higher at the bottom (diffusivity between the bottom layer and the ocean) than for the RL_Sim1 simulation with only molecular diffusion (D_m) + the mixed length diffusion coefficient (D_{MLD}) (refer 2.1 and Fig. 5).

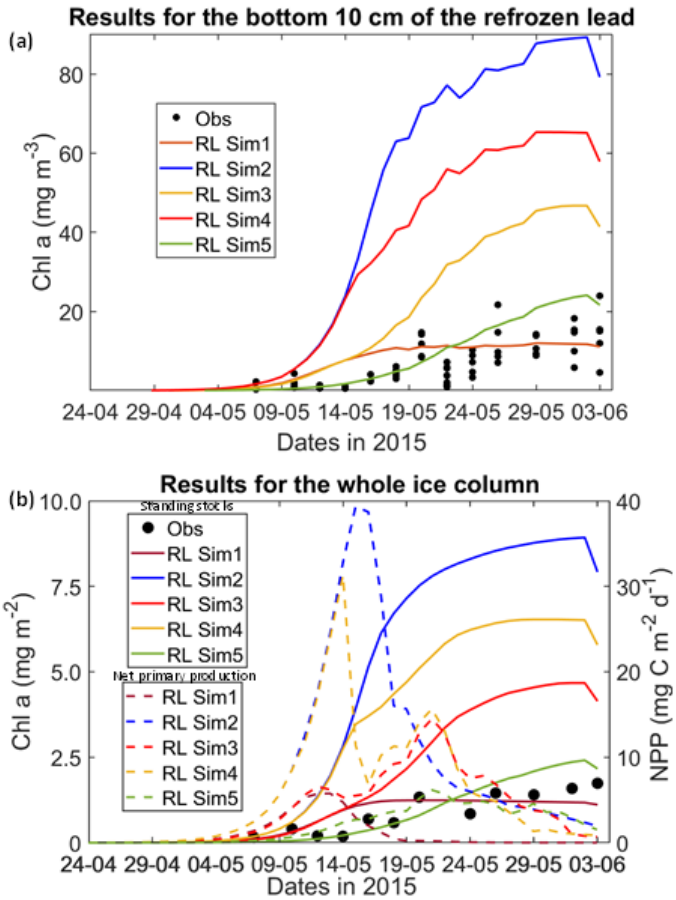

Figure 1. Daily averaged results for the refrozen lead (RL): (a) Observed and modelled *Chl a* concentration values averaged for the ice bottom 10 cm; (b) Observed and modelled *Chl a* standing stock (continuous lines) and modelled net primary production (NPP) (dashed lines) for the whole ice column (refer to Table 1 for details about model simulations). Observations are the same presented in Duarte et al. (2017).

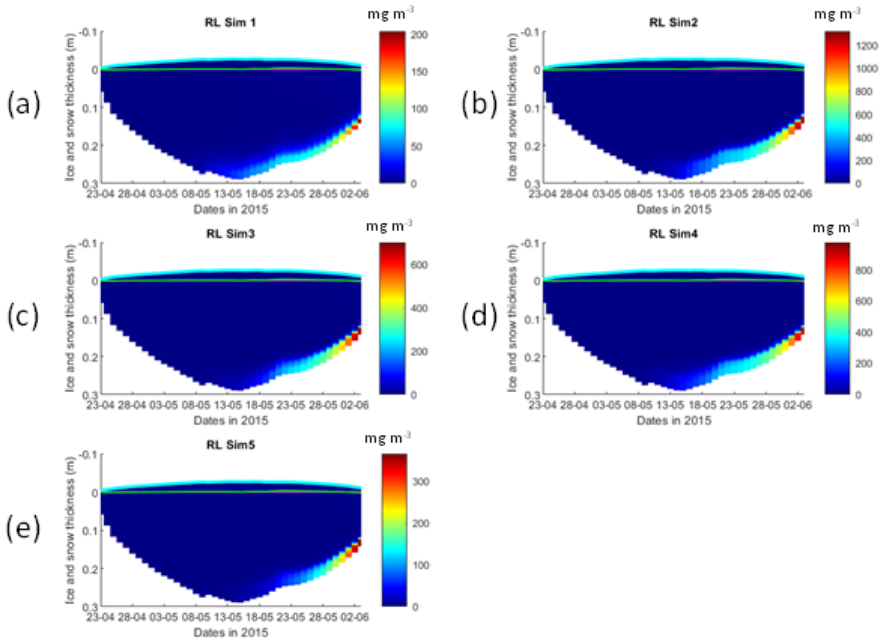

Figure 2. Daily averaged results for the refrozen lead (RL) simulations 1 - 5: Simulated evolution of ice algae *Chl a* as a function of time and depth in the ice (note the colour scale differences between the various panels). Ice thickness is given by the distance between the upper and the lower limits of the maps. The upper regions of the graphs, above the green line with zero values, are above the CICE biogrid and have no brine network. The magenta line, partly covered by the green line, represents sea level. Refer to Table 1 for details about model simulations.

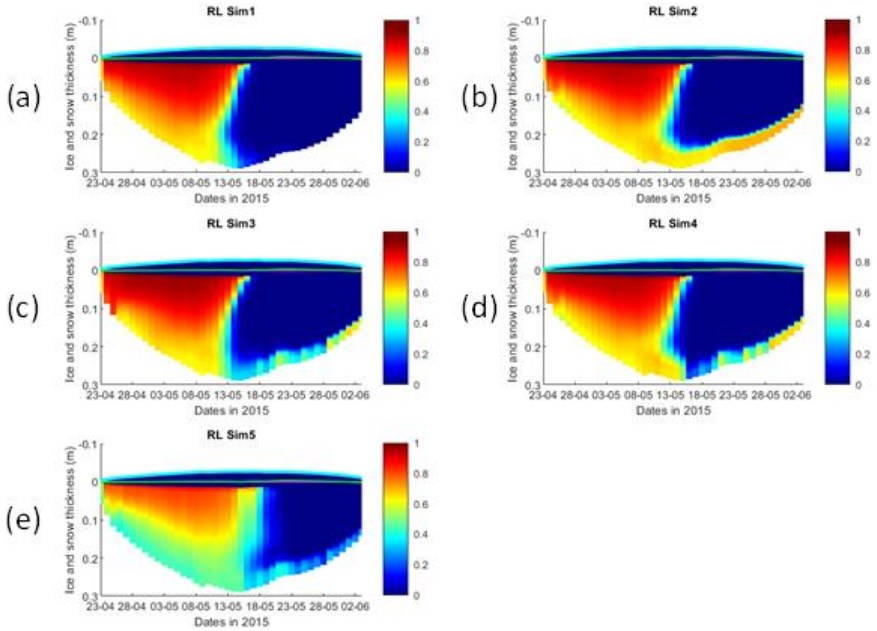

Figure 3. Daily averaged results for the refrozen lead (RL) simulations 1 - 5: Simulated evolution of silicate limitation (one means no limitation and zero is maximal limitation), as a function of time and depth in the ice. Ice thickness is given by the distance between the upper and the lower limits of the maps. The upper regions of the graphs, above the green line with zero values, are above the CICE biogrid and have no brine network. The magenta line, partly covered by the green line,represents sea level. Refer to Table 1 for details about model simulations.

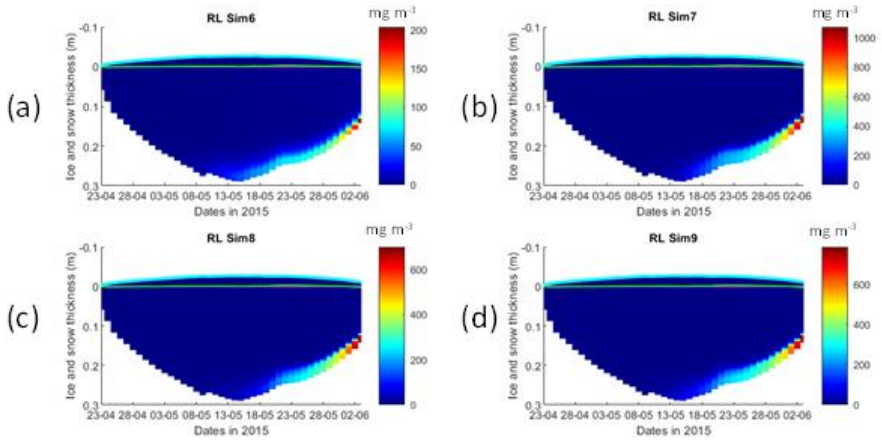

Figure 4. Daily averaged results for the refrozen lead (RL) simulations 6 - 9: Simulated evolution of ice algae *Chl a* as a function of time and depth in the ice (note the colour scale differences between the various panels). Ice thickness is given by the distance between the upper and the lower limits of the maps. The upper regions of the graphs, above the green line with zero values, are above the CICE biogrid and have no brine network. The magenta line, partly covered by the green line, represents sea level. Refer to Table 1 for details about model simulations.

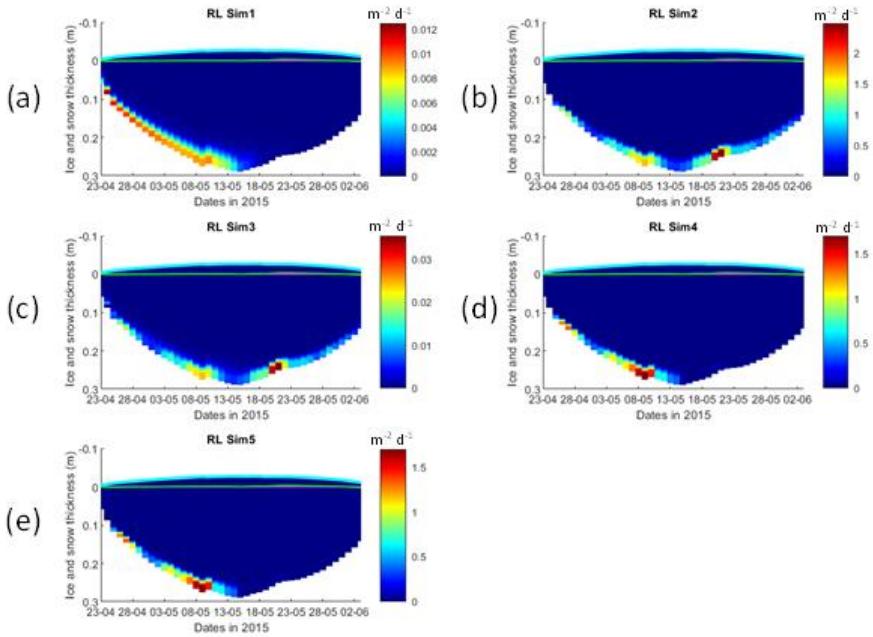

Figure 5. Daily averaged results for the refrozen lead (RL) simulations 1-5: Simulated evolution of interface diffusivity as a function of time and depth in the ice (note the colour scale differences between the various panels). Ice thickness is given by the distance between the upper and the lower limits of the maps. The upper regions of the graphs, above the green line with zero values, are above the CICE biogrid and have no brine network. The magenta line represents sea level. Refer to Table 1 for details about model simulations.

3.2 Second year ice simulations

Simulations with turbulent diffusion (SYI_Sim2 and 3), predict only slightly higher standing stocks and net primary production than with the standard molecular diffusion formulation (SYI_Sim1) (Fig. 6). The visual fit to the standing stock observations is comparable between the various simulations. Changing the half saturation constant for silicate limitation from 2.2 to 4.0 μM has no impact on model results. This is confirmed by analysing the evolution of *Chl a* concentration as a function of time and depth in the ice (Fig. 7), with only minor differences being apparent towards the end of the simulation, when *Chl a* increases

at the bottom layers in the simulations with turbulent diffusion (SYI_Sim 2 and 3). Ice thickness, temperature and salinity profiles are extremely similar among these simulations (Fig. S13).

The dominant limiting factor in these simulations is light, followed by silicate (compare Fig. 8a, c and e with 8b, d and f and with Fig. S14). Light limitation is less severe after the onset of snow and ice melting at the beginning of June. Silicate limitation is very strong above the bottom ice. Nitrogen limitation is highest at a depth range between ~0.4 ~0.7 m below the ice top, with a large overlap with the depth range where a *Chl a* maximum is observed (Fig. 7). Maximal *Chl a* concentration predicted for the RL_Sim1 and RL_Sim5 simulations - those closer to observations - are two orders of magnitude higher than those predicted for SYI (Fig. 2a and e versus Fig. 7). However, standing stocks predicted for RL_Sim1 and RL_Sim5 simulations are smaller than for SYI simulations, as confirmed by the observations (Figs. 1b and 6). Opposite to what was described for the RL simulations, silicate limitation becomes more severe than light limitation at the bottom layer only in SYI_Sim_1, at the beginning of June, close to the end of the simulation (Fig. S15).

Results obtained without algal exchanges between the ocean and the ice (SYI_Sim4 and 5, see Table 1), show the same patterns of those observed with SYI_Sim1 and 2, respectively (Fig. 9 versus Fig. 7, Fig. S17 versus Fig. 8, Figs. S18 versus S14a - d and Figs. S16 versus S13a - d).

Interface diffusivity (one of CICE diagnostic variables, see above) for simulations with turbulent bottom exchanges are up to four orders of magnitude higher at the bottom ice than for simulations with only molecular diffusion (Fig. S19, showing a comparison between SYI_Sim1 and SYI_Sim2).

SYI_Sim1 and 2 were repeated with varying snow thickness (Table 1 and Figs. 10 and 11). In the former simulation (Fig. 10a), as snow height decreases, there is a reduction in light limitation and a sharp increase in silicate limitation, overtaking light limitation (values becoming lower) as early as mid-May. In the latter simulation (Fig. 10b), light limitation prevails irrespective of snow height, except in the case of the lower snow height of 15 cm where silicate becomes more limiting towards the end of the simulation. With the decrease in snow height, there is an increase in *Chl a* concentration in all simulations. Highest values for SYI_Sim2 are ~one order of magnitude larger than those for SYI_Sim1. Moreover, the decrease in snow heights is followed by an earlier and more intense bottom ice algal bloom.

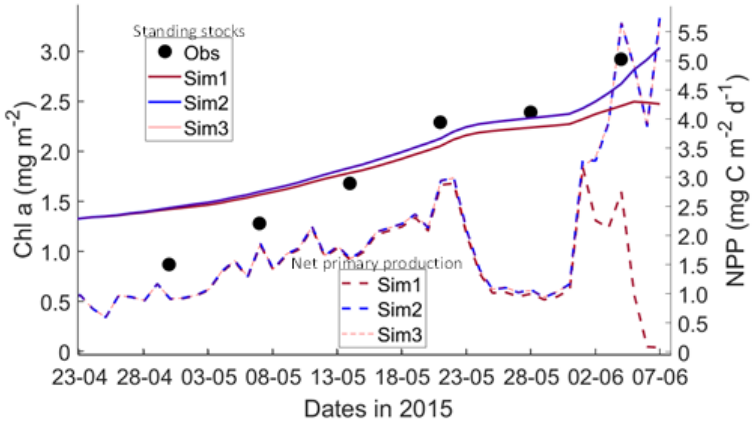

Figure 6. Daily averaged results for second year ice (SYI) simulations 1 - 3: Observed [same data presented in Duarte et al. (2017)] and modelled *Chl a* standing stock (continuous lines) and modelled net primary production (NPP) (dashed lines) for the whole ice column (refer to Table 1 for details about model simulations).

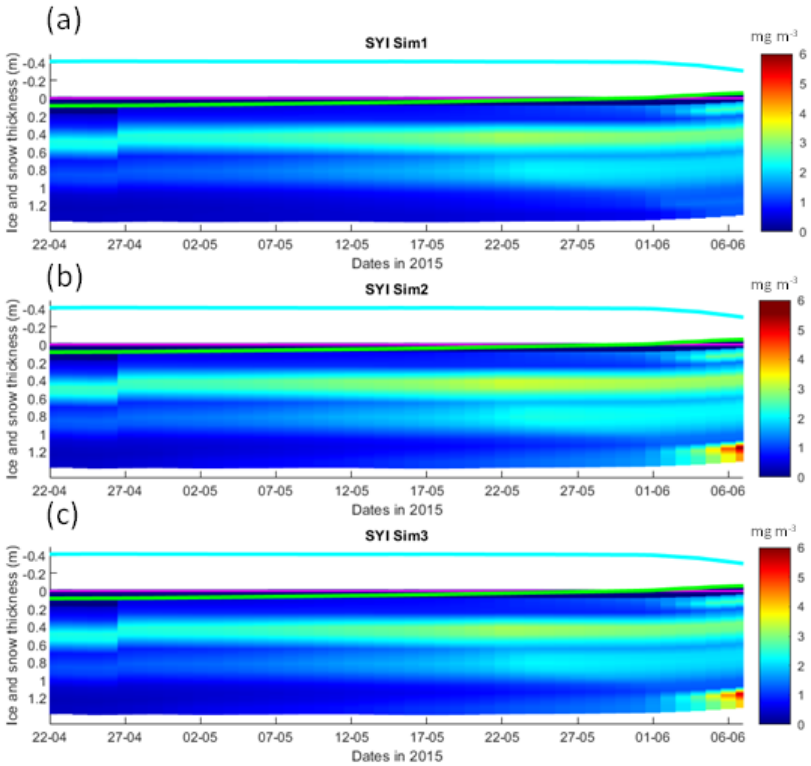

Figure 7. Daily averaged results for second year ice (SYI) simulations 1 - 3: Simulated evolution of ice algae *Chl a* as a function of time and depth in the ice. The upper regions of the graphs, above the green line with zero values, are above the CICE biogrid and have no brine network. The magenta line represents sea level, and the cyan line represents the top of the snow layer. Refer to Table 1 for details about model simulations.

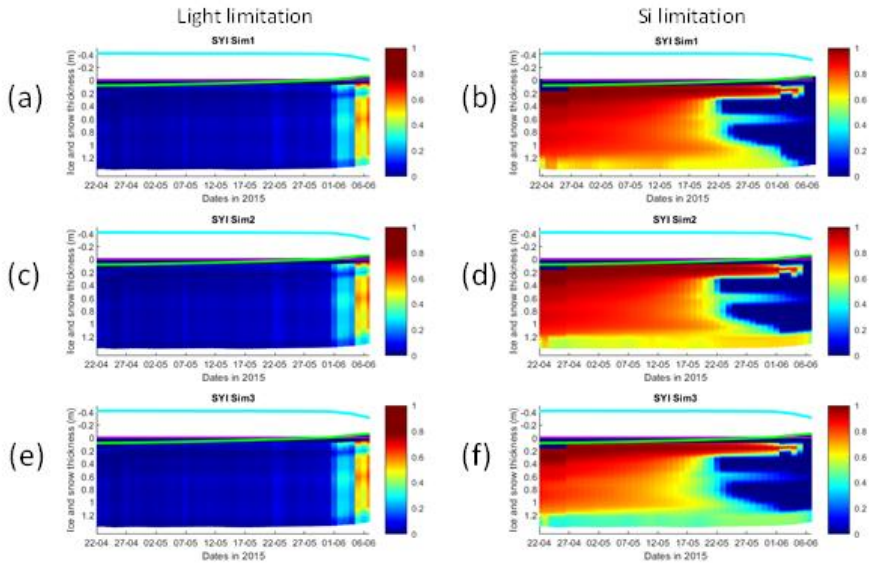

Figure 8. Daily averaged results for second year ice (SYI) simulations 1 - 3: Simulated evolution of light (left panels) and silicate (right panels) limitation (one means no limitation and zero is maximal limitation), as a function of time and depth in the ice. The upper regions of the graphs, above the green line with zero values, are above the CICE biogrid and have no brine network. The magenta line represents sea level, and the cyan line represents the top of the snow layer. Refer to Table 1 for details about model simulations.

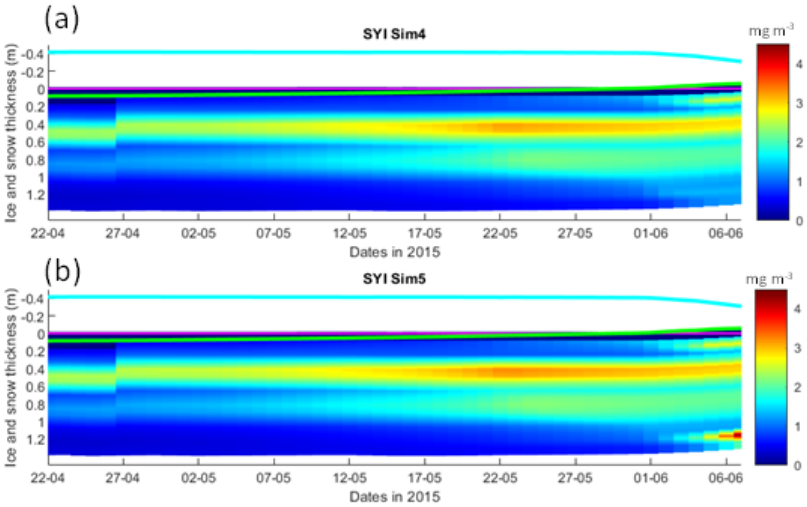

Figure 9. Daily averaged results for second year ice (SYI) simulations 4 and 5: Simulated evolution of ice algae *Chl a* as a function of time and depth in the ice. The upper regions of the graphs, above the green line with zero values, are above the CICE biogrid and have no brine network. The magenta line represents sea level, and the cyan line represents the top of the snow layer. Refer to Table 1 for details about model simulations.

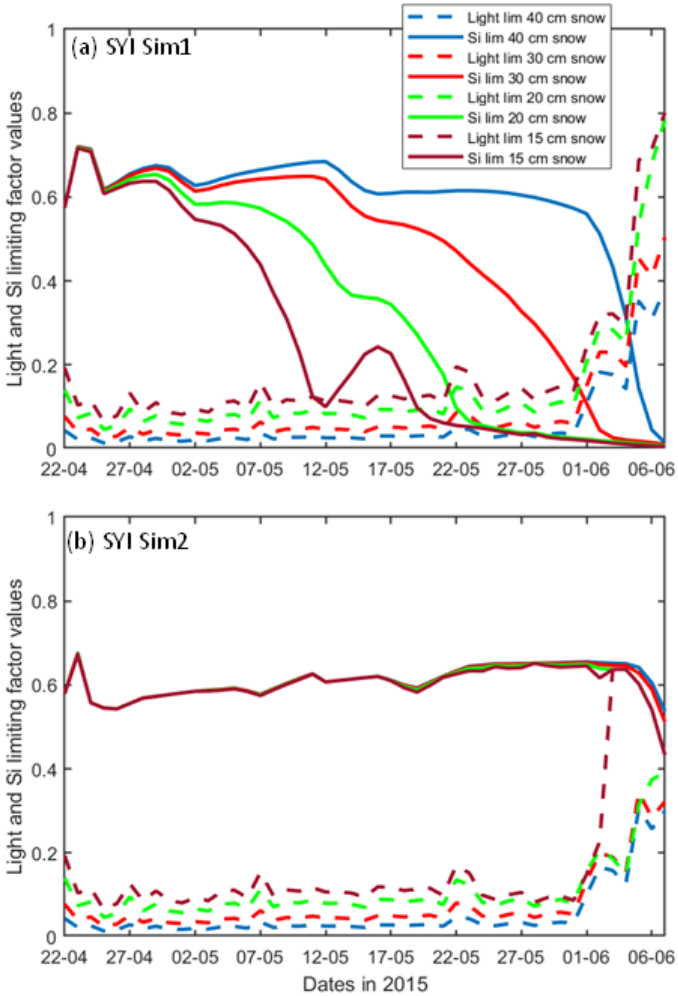

Figure 10. Daily averaged results for the second-year ice (SYI) simulations 1 (a) and 2 (b) starting with a snow depth of 40 (default simulation), 30, 20 and 15 cm: Simulated evolution of light (dashed lines) and silicate (continuous lines) limitation (one means no limitation and zero is maximal limitation), as a function of time at the ice bottom layer (one means no limitation). Refer to Table 1 for details about model simulations.

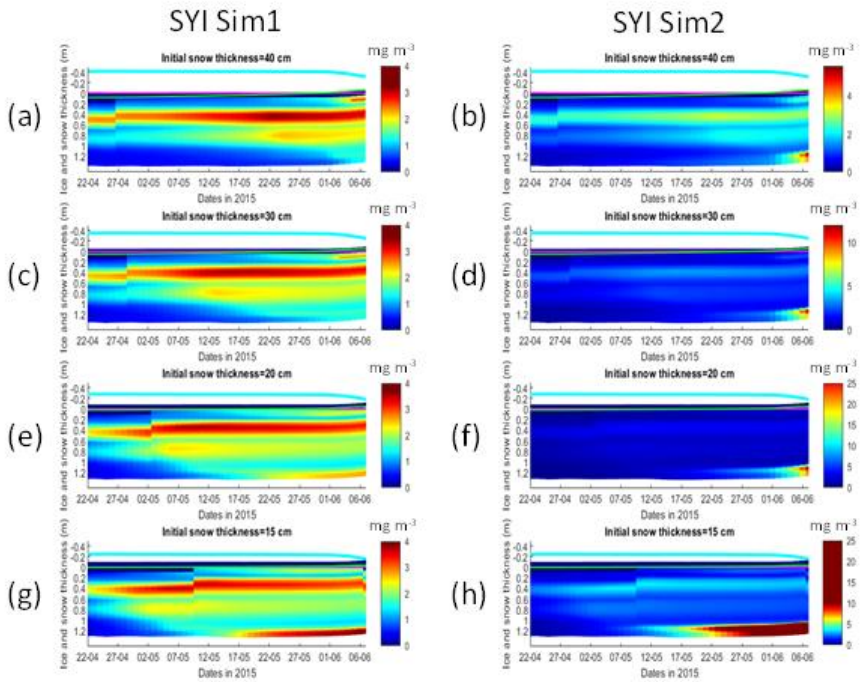

Figure 11. Daily averaged results for second year ice (SYI) simulations 1 (left panels) and 2 (right panels) starting with a snow depth of 40 (default simulation), 30, 20 and 15 cm: Simulated evolution of ice algae *Chl a* as a function of time and depth in the ice. The upper regions of the graphs, above the green line with zero values, are above the CICE biogrid and have no brine network. The magenta line represents sea level, and the cyan line represents the top of the snow layer. Refer to Table 1 for a description of model simulations.

4. Discussion

The results obtained in this study support the initial hypothesis, showing that considering the role of velocity shear on turbulent nutrient exchanges between the ocean and the sea ice, formulated in a way consistent with heat exchanges, leads to a reduction in nutrient limitation that supports a significant increase in ice algal net primary production and *Chl a* biomass accumulation in the bottom ice layers, when production is nutrient limited. Therefore, our results are in line with empirical evidence provided by Cota et al. (1987) and Dalman et al. (2019) but, to the best of our knowledge, experimental evidence from properly designed experiments is still lacking to test our hypothesis. Moreover, our results do not imply necessarily that experiments carried out

with other sea-ice models would render the same trends. The implementation of turbulent mixing considerably relieved silicate limitation in the RL simulations, leading to an increase in NPP, in the duration of the algal growth period, in bottom *Chl a* concentration and in-ice light absorption, increasing light limitation due to shelf-shading [in the CICE model, optical ice properties are influenced by ice algal concentrations (Jeffery et al., 2016)].

In the N-ICE2015 biogeochemical dataset (Assmy et al., 2016), the median of dissolved inorganic nitrogen to silicate ratios in all surface and subsurface water masses, is above 1.7 (unpublished data), which is the upper limit for the nitrogen to silicate ratio for polar diatoms (e.g. Takeda, 1998; Krause et al. 2018). Therefore, it can be expected that, in the region covered by the N-ICE2015 expedition, silicate is more limiting than nitrogen for the production yields of the pennate diatoms characteristic of the bottom-ice communities [the dominant algal functional group in bottom ice, e.g. Leu et al. (2015), van Leeuwe et al. (2019)]. Elsewhere in the Arctic the opposite may be true, considering nitrate and silicate concentrations presented in Leu et al. (2015) and the number of process studies documenting such limitation [e.g., Campbell et al. (2016)]. However, the conclusions taken here about the effects of turbulent mixing are independent of the limiting nutrient.

Implementing turbulent diffusion between the ice and the ocean has obvious implications for model tuning. Our results for the RL show that with this formulation it was necessary to increase the half saturation constant for silicate uptake and to reduce the ocean concentration of algal nitrogen (algalN), reducing the colonization of bottom ice by ice algae, to obtain *Chl a* values comparable to those observed (RL_Sim5). Therefore, whereas Duarte et al. (2017) had to reduce silicate limitation to improve the fit between modelled and observational data, the opposite approach was required when using turbulent diffusion in line with results reported in Lim et al. (2019) for Antarctic sea ice diatoms. This is an example of how one can get good model results by the wrong reasons with difficult to predict consequences on model forecasts under various scenarios.

In the SYI case, only a minor increase in bottom *Chl a* concentration was observed towards the end of simulations SYI_Sim_2 and SYI_Sim_3, when light limitation due to the thick snow cover was relieved by snow melt. Silicate limitation was not as severe as in SYI_Sim_1, due to greater bottom exchanges in the former simulations. The importance of snow cover in controlling ice algal phenology has been stressed before [e.g., Campbell et al. (2015), Leu et al. (2015)].

Duarte et al. (2017) used the delta-Eddington parameter, corresponding to the standard deviation of the snow grain size (R_snow) (Urrego-Blanco et al., 2016), to tune model predicted shortwave radiation at the ice bottom. However, there was still a positive shortwave model bias in June. Therefore, our conclusion about the main limiting role of light in SYI is conservative. Moreover, in part of SYI cores sampled during the N-ICE2015 expedition, in the period covered by our simulations, with an unusually high snow thickness (~40 cm), there was no *Chl a* bottom maximum (Duarte et al., 2017; Olsen et al., 2017).

The dominant role of light limitation in SYI was confirmed in the simulations with reduced snow thickness and alleviated light limitation, with a bottom-ice algal *Chl a* maximum emerging earlier at snow thickness ≤ 20 cm. The reduction of snow thickness had a much larger effect in increasing *Chl a* concentration at the bottom layer when turbulent mixing was used, due to lower silicate limitation. Reducing snow thickness led to a relatively early shift from light to silicate limitation when we used molecular and mixed length diffusion, whereas this shift occurred only at the very end of the simulated period when we

used turbulent diffusion at the ice-ocean interface, driven by velocity shear, instead of molecular diffusion. The effects of different types of diffusion, upon reduction of the snow cover and the possible development of a bottom ice algal bloom, are critical aspects when simulating ice algal phenology and attempting to quantify the contribution of sea ice algae to Arctic primary production.

Simulated shear-driven turbulent diffusivities are up to four orders of magnitude higher than molecular + mixed length diffusivities at the bottom ice and the results presented herein emphasize their potential role in sea ice biogeochemistry. The number and intensity of Arctic winter storms has increased over the 1979–2016 period (Rinke et al., 2017; Graham et al., 2017) and the effect of more frequent and more intensive winter storms in the Atlantic Sector of the Arctic Ocean is a thinner, weaker, and younger snow-laden ice pack (Graham et al., 2019). Storms that occur late in the winter season, after a deep snowpack has accumulated, have the potential to promote ice growth by dynamically opening leads where new ice growth can take place. The young ice of the refrozen leads does not have time to accumulate a deep snow layer until the melting season, which could lead to light limitation of algal growth. All things considered, it can be expected that ongoing trends in the Arctic will lead to a release from light limitation in increasingly larger areas of the ice pack in late winter, which will lead to more likely nutrient limitation earlier in spring (e.g. Lannuzel et al. 2020). These effects will be further amplified under thinning of the snowpack as observed in western Arctic, and in the Beaufort and Chukchi seas, over the last decades (Webster et al., 2014). Therefore, properly parameterizing nutrient exchanges between the ice and the ocean in sea-ice biogeochemical models is of utmost importance to avoid overestimating nutrient limitation and thus underestimating sea ice algal primary production.

In existing sea-ice models there are "natural" differences between the way budgets for non-conservative tracers such as nutrients are closed compared to those of heat and salt, which are related to the biogeochemical sinks and sources (e.g., equation 18 in Vancoppenolle et al., 2010), but also some "inconsistencies", related with the way their transfers between the ocean and the ice are computed. Interestingly, some models (e.g., Jin et al., 2006, 2008 and Hunke et al., 2016) apply the diffusion equation to calculate exchanges across the bottom ice not only to dissolved tracers, but also to algal cells. This is to guarantee a mechanism of ice colonization by microalgae. However, the usage of the same coefficient for dissolved and particulate components creates significant uncertainty.

Molecular diffusion is a slow process compared with turbulent exchanges. This justifies the usage of diffusion coefficients which are much higher than molecular diffusivity, as in Jin et al. (2006), using a value of 1.0 10^{-5} m^2 s^{-1}, four orders of magnitude higher than the value indicated in Mann and Lazier (2005) – 1.5 10^{-9} m^2 s^{-1} – or the parameterization of molecular diffusivity as a function of friction velocity as in Mortenson et al. (2017). The approach proposed herein, formulating bottom-ice nutrient exchanges in a way that is consistent with heat exchanges, provides a physically sound, consistent, and easy to implement alternative.

Calculating diffusion fluxes across the molecular sublayer may be challenging, since it is necessary to estimate the boundary concentrations of this layer, which is only a few tenths of millimetre thick (e.g. Lavoie et al., 2005). This implies resolving with a great detail the ocean surface layer (*sensu* MacPhee, 2008), which is not practical with standalone sea ice models but doable with coupled ocean-sea ice models. Moreover, one needs to know whether exchanges of heat, salt and nutrients are

Formatted: Superscript

Formatted: Superscript

dominated by molecular exchange or by turbulent exchange. This may be challenging on its own since it depends not only on knowing friction velocities but also on knowing the roughness of the bottom ice (e.g. Olsen et al.2019). Ideally, when using coupled ocean-sea ice models, and assuming it is practical to estimate the type of dominant exchanges, one may use either the approach described by Lavoie et al. (2005) or the approach described herein based on McPhee (2008) and grounded on experimental work. Whatever the case, it seems rather likely that we still lack the measurements to properly evaluate these various approaches and find an optimal solution. The way forward implies the availability of eddy covariance data for 3D current velocity, temperature, salinity and ideally, a limiting nutrient, collected at the sea ice-ocean interface over periods of sea ice growth and melting. Such data should be accompanied by vertical profiles for the same tracers, at high resolution, across the surface and the mixing layers (*sensu* McPhee, 2008) and by sea ice bottom samples. Such experiments may be carried out in the sea and in sea ice laboratories under controlled conditions, and they will help to evaluate the results presented herein and improving the parameterizations used in models for the sea ice-ocean interface. Another layer of complexity are the effects of sea ice ridges and keels on the turbulent exchange coefficients (Tsamados et al., 2014). According to these authors such effects are important for regional sea ice modelling, which reinforces the need of experimental studies of the type mentioned above.

5. Conclusions

Considering the role of velocity shear on turbulent nutrient exchanges at the interface between the ocean and the ice in a sea-ice biogeochemical sub-model, leads to a reduction in nutrient limitation and a significant increase in ice algal net primary production and *Chl a* biomass accumulation in the bottom-ice layers, when production is nutrient limited. The results presented herein emphasize the potential role of bottom-ice nutrient exchange processes, irrespective of brine dynamics and other physical-chemical processes, in delivering nutrients to bottom-ice algal communities, and thus the importance of properly including them in sea-ice models. The relevance of this becomes even more apparent considering ongoing changes in the Arctic icescape, with a predictable decrease in light limitation as ice becomes thinner and more fractured, with an expected reduction in snow cover.

Code availability

The software code used in this study may be found at:
https://doi.org/10.5281/zenodo.4675097 and ~~https://doi.org/10.5281/zenodo.4675021~~
https://doi.org/10.5281/zenodo.5795034
This code is in a fork derived from the CICE Consortium repository (https://github.com/CICE-Consortium).

The Consortium's codes are open-source with a standard 3-clause BSD license and are is under the following Copyright license, available at (https://cice-consortium-cice.readthedocs.io/en/master/intro/copyright.html)

Data availability

Model forcing function files may be found at: https://doi.org/10.5281/zenodo.4672176

Results from model simulations described above, in the form of CICE daily netCDF history files iceh.* may be found at: http://doi.org/10.5281/zenodo.4672210

There is one directory for each simulation, and it includes besides the historical files the input file (ice_in) with the simulation parameters.

Authors contribution

Pedro Duarte made the software changes, designed the experiments, performed the simulations and prepared the manuscript with contributions from all co-authors.

Philipp Assmy contributed to the writing of the manuscript.

Karley Campbell contributed to the writing of the manuscript.

Arild Sundfjord contributed to the writing of the manuscript and to funding acquisition.

Competing interests

The authors declare that they have no conflict of interest.

Acknowledgements

This work has been supported by the Fram Centre Arctic Ocean flagship project "Mesoscale physical and biogeochemical modelling of the ocean and sea-ice in the Arctic Ocean" (project reference 66200), the Norwegian Metacenter for Computational Science application "NN9300K - Ecosystem modelling of the Arctic Ocean around Svalbard", the Norwegian "Nansen Legacy" project (no. 276730) and the European Union's Horizon 2020 research and innovation programme under grant agreement No 869154 (project FACE-IT). Contributions by K Campbell are supported by the Diatom ARCTIC project (NE/R012849/1;03F0810A), part of the Changing Arctic Ocean program, jointly funded by the UKRI Natural Environment Research Council and the German Federal Ministry of Education and Research (BMBF).

References

Arrigo, K. R., Kremer, J. N., and Sullivan, C. W.: A Simulated Antarctic Fast Ice Ecosystem, J. Geophy. Res, 98, 17, 1993.

Assmy, P., Duarte, P., Dujardin, J., Fernández-Méndez, M., Fransson, A., Hodgson, R., Kauko, H., Kristiansen, S., Mundy, C. J., Olsen, L. M., Peeken, I., Sandbu, M., Wallenschus, J., Wold, A.: N-ICE2015 water column biogeochemistry [Data set], Norwegian Polar Institute, https://doi.org/10.21334/npolar.2016.3ebb7f64, 2017.

Assmy, P., Dodd, P. A., Duarte, P., Dujardin, J., Elliott, A., Fernández-Méndez, M., Fransson, A., Granskog, M. A., Hendry, K., Hodgson, R., Kauko, H., Kristiansen, S., Leng, M. J., Meyer, A., Mundy, C. J., Olsen, L. M., Peeken, I., Sandbu, M., Wallenschus, J., Wold, A.: N-ICE2015 sea ice biogeochemistry [Data set], Norwegian Polar Institute, https://doi.org/10.21334/npolar.2017.d3e93b31, 2017.

Brzezinski, M. A.: The Si-C-N Ratio of Marine Diatoms - Interspecific Variability and the Effect of Some Environmental Variables, J. Phycol., 21, 347-357, 1985.

Campbell, K., Mundy, C. J., Barber, D. G. and Gosselin, M.: Characterizing the sea ice algae chlorophyll a–snow depth relationship over Arctic spring melt using transmitted irradiance, J. Mar. Sys., 147, 76-84, doi: https://doi.org/10.1016/j.jmarsys.2014.01.008, 2015.

Campbell, K., Mundy, C. J., Landy, J. C., Delaforge, A., Michel, C. and Rysgaard, S.: Community dynamics of bottom-ice algae in Dease Strait of the Canadian Arctic. Prog. Oceanogr., 149, 27-39, doi: http://dx.doi.org/10.1016/j.pocean.2016.10.005, 2016.

Carmack, E.: Circulation and Mixing in Ice-Covered Waters, in: The Geophysics of Sea Ice. NATO ASI Series (Series B: Physics), edited by Untersteiner N. Springer, Boston, MA. 641-712, https://doi.org/10.1007/978-1-4899-5352-0_11, 1986.

Cota, G. F., Prinsenberg, S. J., Bennett, E. B., Loder, J. W., Lewis, M. R., Anning, J. L., Watson, N. H. F., and Harris, L. R.: Nutrient Fluxes during Extended Blooms of Arctic Ice Algae, J. Geophys. Res.-Oceans, 92, 1951-1962, doi: 10.1029/Jc092ic02p01951, 1987.

Cota, G. F., and Horne, E. P. W.: Physical Control of Arctic Ice Algal Production, Mar. Ecol. Prog. Ser., 52, 111-121, doi: 10.3354/meps052111, 1989.

Cota, G. F., and Sullivan, C. W.: Photoadaptation, Growth and Production of Bottom Ice Algae in the Antarctic, J. Phycol., 26, 399-411, doi: 10.1111/j.0022-3646.1990.00399.x, 1990.

Dalman, L. A., Else, B. G. T., Barber, D., Carmack, E., Williams, W. J., Campbell, K. , Duke, P. J., Kirillov, S., and Mundy, C. J.: Enhanced bottom-ice algal biomass across a tidal strait in the Kitikmeot Sea of the Canadian Arctic, Elem. Sci. Anth., 7, doi: https://doi.org/10.1525/elementa.361, 2019.

Duarte, P., Meyer, A., Olsen, L. M., Kauko, H. M., Assmy, P., Rosel, A., Itkin, P., Hudson, S. R., Granskog, M. A., Gerland, S., Sundfjord, A., Steen, H., Hop, H., Cohen, L., Peterson, A. K., Jeffery, N., Elliott, S. M., Hunke, E. C., and Turner, A. K.: Sea ice thermohaline dynamics and biogeochemistry in the Arctic Ocean: Empirical and model results, J. Geophys. Res.-Biogeosciences, 122, 1632-1654, doi: 10.1002/2016JG003660, 2017.

Duarte, P.: CICE-Consortium/Icepack: Icepack with bottom drag, heat and nutrient turbulent diffusion (Version 1.1). Zenodo. http://doi.org/10.5281/zenodo.4675021, (2021a, April 9).

Duarte, P.: CICE-Consortium/CICE: CICE with bottom drag, heat and nutrient turbulent diffusion (Version 1.1). Zenodo. http://doi.org/10.5281/zenodo.4675097, (2021b, April 9).

Duarte, P.: The importance of turbulent ocean-sea ice nutrient exchanges for simulation of ice algal biomass and production with CICE6.1 and Icepack 1.2 - CICE forcing files (Version v1.0) [Data set]. Zenodo. http://doi.org/10.5281/zenodo.4672176, 2021c.

Duarte, P.: The importance of turbulent ocean-sea ice nutrient exchanges for simulation of ice algal biomass and production with CICE6.1 and Icepack 1.2 - model simulations (Version v1.0) [Data set]. Zenodo. http://doi.org/10.5281/zenodo.4672210, 2021c.

Gerland, S., Granskog, M. A., King, J, Rösel, A.: N-ICE2015 Ice core physics: temperature, salinity and density [Data set], Norwegian Polar Institute, https://doi.org/10.21334/npolar.2017.c3db82e3, 2017.

Gosselin, M., Legendre, L., Demers, S., and Ingram, R. G.: Responses of Sea-Ice Microalgae to Climatic and Fortnightly Tidal Energy Inputs (Manitounuk Sound, Hudson-Bay), Can. J. Fish. Aquat. Sci., 42, 999-1006, doi: 10.1139/f85-125, 1985.

Graham, R. M., Rinke, A., Cohen, L., Hudson, S. R., Walden, V. P., Granskog, M. A., Dorn, W., Kayser, M., and Maturilli, M.: A comparison of the two Arctic atmospheric winter states observed during N-ICE2015 and SHEBA, J. Geophys. Res.-Atmospheres, 122, 5716-5737, doi: 10.1002/2016JD025475, 2017.

Graham, R. M., Itkin, P., Meyer, A., Sundfjord, A., Spreen, G., Smedsrud, L. H., Liston, G. E., Cheng, B., Cohen, L., Divine, D., Fer, I., Fransson, A., Gerland, S., Haapala, J., Hudson, S. R., Johansson, A. M., King, J., Merkouriadi, I., Peterson, A. K., Provost, C., Randelhoff, A., Rinke, A., Rosel, A., Sennechael, N., Walden, V., Duarte, P., Assmy, P., Steen, H., and Granskog, M. A.: Winter storms accelerate the demise of sea ice in the Atlantic sector of the Arctic Ocean, Sci. Rep.-Uk, 9, Artn 9222, doi: 10.1038/S41598-019-45574-5, 2019.

Granskog, M. A., Fer, I., Rinke, A., and Steen, H.: Atmosphere-Ice-Ocean-Ecosystem Processes in a Thinner Arctic Sea Ice Regime: The Norwegian Young Sea ICE (N-ICE2015) Expedition, J. Geophys. Res.-Oceans, 123, 1586-1594, doi: 10.1002/2017jc013328, 2018.

Hegseth, E. N.: Sub-Ice Algal Assemblages of the Barents Sea - Species Composition, Chemical-Composition, and Growth-Rates, Polar. Biol., 12, 485-496, 1992.

Hudson, S. R., Cohen, L., Walden, V.: N-ICE2015 surface meteorology [Data set], Norwegian Polar Institute, https://doi.org/10.21334/npolar.2015.056a61d1, 2015.

Hudson, S. R., Cohen, L., Walden, V.:,N-ICE2015 surface broadband radiation data [Data set], Norwegian Polar Institute, https://doi.org/10.21334/npolar.2016.a89cb766, 2016.

Hunke, E. C., Lipscomb, W. H., Turner, A. K., Jeffery, N., Elliot, S.: CICE: the Los Alamos Sea Ice Model. Documentation and User's Manual Version 5.1. Los Alamos National Laboratory, USA. LA-CC-06-012, 2015.

Ingram, R. G., Osler, J. C., and Legendre, L.: Influence of Internal Wave-Induced Vertical Mixing on Ice Algal Production in a Highly Stratified Sound, Estuar. Coast. Shelf. S., 29, 435-446, doi: 10.1016/0272-7714(89)90078-4, 1989.

Jeffery, N., Hunke, E. C., and Elliott, S. M.: Modeling the transport of passive tracers in sea ice, J. Geophys. Res.-Oceans, 116, Artn C07020, doi:10.1029/2010jc006527, 2011.

Jeffery, N., Elliott, S., Hunke, E. C., Lipscomb, W. H., Turner, A. K.: Biogeochemistry of CICE: The Los Alamos Sea Ice Model, Documentation and User's Manual. Zbgc_colpkg modifications to Version 5, Los Alamos National Laboratory, Los Alamos, N. M., 2016.

Jin, M., Deal, C. J., Wang, J., Shin, K. H., Tanaka, N., Whitledge, T. E., Lee, S. H., and Gradinger, R. R.: Controls of the landfast ice–ocean ecosystem offshore Barrow, Alaska, Ann. Glaciol., 44, 9, 2006.

Jin, M., Deal, C., and Jia, W.: A coupled ice-ocean ecosystem model for I-D and 3-D applications in the Bering and Chukchi Seas, Chinese Journal of Polar Science, 19, 11, 2008.

Krause, J. W., Duarte, C. M., Marquez, I. A., Assmy, P., Fernandez-Mendez, M., Wiedmann, I., Wassmann, P., Kristiansen, S., and Agusti, S.: Biogenic silica production and diatom dynamics in the Svalbard region during spring, Biogeosciences, 15, 6503-6517, doi: 10.5194/bg-15-6503-2018, 2018.

Lake, R. A, Lewis, E. L.: Salt rejection by sea ice during growth, J.Geophys. Res., 75, 583-597, 1970.

Lannuzel, D., Tedesco, T., van Leeuwe, M., Campbell, K., Flores, H., Delille, B., Miller, L., Stefels, J., Assmy, P., Bowman, J., Brown, K., Castellani, G., Chierici, M., Crabeck, O., Damm, E., Else, B., Fransson, A., Fripiat, F., Geilfus, N. X., Jacques, C., Jones, E., Kaartokallio, H., Kotovitch, M., Meiners, K., Moreau, S., Nomura, D., Peeken, I., Rintala, J. M., Steiner, N., Tison, J. L., Vancoppenolle, M., Van der Linden, F., Vichi, M. and Wongpan, P.: The future of Arctic sea-ice biogeochemistry and ice-associated ecosystems, Nat. Clim. Change 10(11), 983-992, doi: https://doi.org/10.1038/s41558-020-00940-4, 2020.

Lavoie, D., Denman, K., and Michel, C.: Modeling ice algal growth and decline in a seasonally ice-covered region of the Arctic (Resolute Passage, Canadian Archipelago), J. Geophys. Res.-Oceans, 110, Artn C11009, doi: 10.1029/2005jc002922, 2005.

Leu, E., Mundy, C. J., Assmy, P., Campbell, K., Gabrielsen, T. M., Gosselin, M., Juul-Pedersen, T., and Gradinger, R.: Arctic spring awakening - Steering principles behind the phenology of vernal ice algal blooms, Progr. Oceanogr., 139, 151-170, doi: 10.1016/j.pocean.2015.07.012, 2015.

Lim, S. M., Moreau, S., Vancoppenolle, M., Deman, F., Roukaerts, A., Meiners, K. M., Janssens, J., and Lannuzel, D.: Field Observations and Physical-Biogeochemical Modeling Suggest Low Silicon Affinity for Antarctic Fast Ice Diatoms, J Geophys Res-Oceans, 124, 7837-7853, 10.1029/2018jc014458, 2019.

Mann, K. H., Lazier, J. R. N.: Dynamics of Marine Ecosystems, Third Edition, Blackwell Publishing Ltd., Carlton, Victoria 3053, Australia, 503p., doi:10.1002/9781118687901, 2005.

McPhee, M.: Air-ice-ocean interaction: Turbulent ocean boundary layer exchange processes. Springer-Verlag, New York, 216p., doi: 10.1007/978-0-387-78335-2, 2008.

McPhee, M. G., Morison, J. H., and Nilsen, F.: Revisiting heat and salt exchange at the ice-ocean interface: Ocean flux and modeling considerations, J. Geophys. Res.-Oceans, 113, Artn C06014, doi: 10.1029/2007jc004383, 2008.

Mortenson, E., Hayashida, H., Steiner, N., Monahan, A., Blais, M., Gale, M. A., Galindo, V., Gosselin, M., Hu, X. M., Lavoie, D., and Mundy, C. J.: A model-based analysis of physical and biological controls on ice algal and pelagic primary production in Resolute Passage, Elem. Sci. Anth., 5, Artn 39, doi:10.1525/Elementa.229, 2017.

Nelson, D. M., and Treguer, P.: Role of Silicon as a Limiting Nutrient to Antarctic Diatoms - Evidence from Kinetic-Studies in the Ross Sea Ice-Edge Zone, Mar. Ecol. Prog. Ser., 80, 255-264, doi: 10.3354/meps080255, 1992.

Niedrauer, T. M., and Martin, S.: Experimental-Study of Brine Drainage and Convection in Young Sea Ice, J. Geophys. Res.-Oceans, 84, 1176-1186, doi: 10.1029/JC084iC03p01176, 1979.

Notz, D., and Worster, M. G.: Desalination processes of sea ice revisited, J Geophys Res-Oceans, 114, Artn C05006, doi: 10.1029/2008jc004885, 2009.

Olsen, L. M., Laney, S. R., Duarte, P., Kauko, H. M., Fernández-Méndez, M., Mundy, C. J., Rösel, A., Meyer, A., Itkin, P., Cohen, L., Peeken, I., Tatarek, A., Różańska, M., Wiktor, J., Taskjelle, T., Pavlov, A. K., Hudson, S. R., Granskog, M. A., Hop, H., and Assmy, P.: The seeding of ice-algal blooms in Arctic pack ice: the multiyear ice seed repository hypothesis, J Geophys Res-Biogeosciences, 122(7), 1529-1548, doi: 10.1002/2016jg003668, 2017.

Olsen, L. M., Duarte, P., Peralta-Ferriz, C., Kauko, H. M., Johansson, M., Peeken, I., Różańska-Pluta, M., Tatarek, A., Wiktor, J., Fernández-Méndez, M., Wagner, P. M., Pavlov, A. K., Hop, H., and Assmy, P.: A red tide in the pack ice of the Arctic Ocean, Sci Rep, 9, 9536, 10.1038/s41598-019-45935-0, 2019.

Peterson, A. K., Fer, I., Randelhoff, A., Meyer, A., Håvik, L., Smedsrud, L. H., Onarheim, L., Muilwijk, M., Sundfjord, A., McPhee, M. G.: N-ICE2015 Ocean turbulent fluxes from under-ice turbulence cluster (TIC) [Data set], Norwegian Polar Institute, https://doi.org/10.21334/npolar.2016.ab29f1e2, 2016.

Reeburgh, W. S.: Fluxes Associated with Brine Motion in Growing Sea Ice, Polar Biol., 3, 29-33, doi: 10.1007/Bf00265564, 1984.

Rinke, A., Maturilli, M., Graham, R. M., Matthes, H., Handorf, D., Cohen, L., Hudson, S. R., and Moore, J. C.: Extreme cyclone events in the Arctic: Wintertime variability and trends, Environ. Res. Letters, 12, Artn 094006, doi:10.1088/1748-9326/Aa7def, 2017.

Smith, R. E. H., Cavaletto, J. F., Eadie, B. J., and Gardner, W. S.: Growth and Lipid-Composition of High Arctic Ice Algae during the Spring Bloom at Resolute, Northwest-Territories, Canada, Mar. Ecol. Prog. Ser., 97, 19-29, doi: 10.3354/meps097019, 1993.

Takeda, S.: Influence of iron availability on nutrient consumption ratio of diatoms in oceanic waters, Nature, 393, 774-777, doi: 10.1038/31674, 1998.

Tedesco, L., Vichi, M.: BFM-SI: a new implementation of the Biogeochemical Flux Model in sea ice. in: CMCC Research Papers, http://www.cmcc.it/publications-meetings/publications/researchpapers/rp0081-ans-03-2010, http://hdl.handle.net/2122/5956, 2010.

Tedesco, L., Vichi, M., and Scoccimarro, E.: Sea-ice algal phenology in a warmer Arctic, Sci. Adv., 5, ARTN eaav4830, doi: 10.1126/sciadv.aav4830, 2019.

Thomas, M., Vancoppenolle, M., France, J. L., Sturges, W. T., Bakker, D. C. E., Kaiser, J., and von Glasow, R.: Tracer Measurements in Growing Sea Ice Support Convective Gravity Drainage Parameterizations, J Geophys Res-Oceans, 125, ARTN e2019JC015791, doi: 10.1029/2019JC015791, 2020.

Turner, A. K., Hunke, E. C., and Bitz, C. M.: Two modes of sea-ice gravity drainage: A parameterization for large-scale modeling, J. Geophys. Res.-Oceans, 118, 2279-2294, doi: 10.1002/jgrc.20171, 2013.

Urrego-Blanco, J. R., Urban, N. M., Hunke, E. C., Turner, A. K., and Jeffery, N.: Uncertainty quantification and global sensitivity analysis of the Los Alamos sea ice model, J. Geophys. Res.-Oceans, 121, 2709-2732, doi: 10.1002/2015JC011558, 2016.

Tsamados, M., Feltham, D. L., Schroeder, D., Flocco, D., Farrell, S. L., Kurtz, N., Laxon, S. W., and Bacon, S.: Impact of Variable Atmospheric and Oceanic Form Drag on Simulations of Arctic Sea Ice*, Journal of Physical Oceanography, 44, 1329-1353, 10.1175/Jpo-D-13-0215.1, 2014.

Vancoppenolle, M., Bitz, C. M., and Fichefet, T.: Summer landfast sea ice desalination at Point Barrow, Alaska: Modeling and observations, J. Geophys. Res.-Oceans, 112, Artn C04022, doi: 10.1029/2006jc003493, 2007.

Vancoppenolle, M., Goosse, H., de Montety, A., Fichefet, T., Tremblay, B., and Tison, J. L.: Modeling brine and nutrient dynamics in Antarctic sea ice: The case of dissolved silica, J Geophys Res-Oceans, 115, Artn C02005, doi: 10.1029/2009jc005369, 2010.

Vancoppenolle, M., Bopp, L., Madec, G., Dunne, J., Ilyina, T., Halloran, P. R., and Steiner, N.: Future Arctic Ocean primary productivity from CMIP5 simulations: Uncertain outcome, but consistent mechanisms, Global Biogeochem Cy, 27, 605-619, doi: 10.1002/gbc.20055, 2013.

van Leeuwe, M. A., Tedesco, L., Arrigo, K. R., Assmy, P., Campbell, K., Meiners, K. M., Rintala, J. M., Selz, V., Thomas, D. N. and Stefels, J.: Microalgal community structure and primary production in Arctic and Antarctic sea ice: A synthesis. Elem. Sci. Anth., 6:4., doi: https://doi.org/10.1525/elementa.267, 2018.

Wakatsuchi, M., and Ono, N.: Measurements of Salinity and Volume of Brine Excluded from Growing Sea Ice, J. Geophys. Res.-Oceans, 88, 2943-2951, doi: 10.1029/JC088iC05p02943, 1983.

Webster, M. A., Rigor, I. G., Nghiem, S. V., Kurtz, N. T., Farrell, S. L., Perovich, D. K. and Sturm, M.: Interdecadal changes in snow depth on Arctic sea ice, J. Geophys. Res.-Oceans 119(8), 5395-5406, doi:10.1002/2014JC009985, 2014.

Wells, A. J., Wettlaufer, J. S., and Orszag, S. A.: Brine fluxes from growing sea ice, Geophys Res Lett, 38, Artn L04501, doi: 10.1029/2010gl046288, 2011.